Divergence of the Variance of the Optical Phase in Gain-Switched Semiconductor Lasers Described by Stochastic Rate Equations

Angel Valle*

Instituto de Física de Cantabria (CSIC–Universidad de Cantabria), Avda. Los Castros s/n, 39005 Santander, Spain

(Received 14 October 2022; revised 24 March 2023; accepted 6 April 2023; published 2 May 2023)

We report a theoretical study of the phase diffusion in a gain-switched single-mode semiconductor laser. We use stochastic rate equations for the electric field to analyze the phase statistics of the gain-switched laser. Their use avoids the instabilities obtained with rate equations for the photon number and optical phase when the photon number is small. However, we show that a new problem appears when the field equations are integrated: the variance of the optical phase becomes divergent. This divergence cannot be observed with the numerical integration of the commonly used equations for the photon number and optical phase because of the previous instabilities. The divergence of the phase variance means that this quantity does not reach a fixed value as the integration time step is decreased. We find that the phase variance increases as the integration time step decreases, with no sign of saturation behavior even for tiny steps. We explain the divergence by making the analogy of our problem with two-dimensional Brownian motion. The fact that the divergence appears is not surprising because in 1940 Paul Lèvy demonstrated that the variance of the polar angle in two-dimensional Brownian motion is a divergent quantity. Our results show that stochastic rate equations for the photon number and phase are not appropriate for describing the phase statistics when the photon number is small. Simulation of the stochastic rate equations for the electric field are consistent with Lèvy's results but gives unphysical results since an infinite value is obtained for a quantity that can be measured.

DOI: 10.1103/PhysRevApplied.19.054005

I. INTRODUCTION

Semiconductor lasers are normally used as single-photon sources in most commercial and research quantum key distribution (QKD) systems [1]. Light pulses with random phases are generated by gain-switching these lasers because of the random character of the phase of the spontaneous-emission photons that seed these pulses during their formation. Weak coherent pulses, obtained from attenuation of semiconductor-laser pulses, have been used as single-photon sources in practical QKD systems since the early 1990s [2]. Another practical application of random-phase pulses emitted by gain-switched semiconductor lasers is quantum random number generation [3–6]. Quantum random number generators (QRNGs) are a particular type of hardware physical random number generator in which the data are obtained from quantum events. Their main advantage is that the randomness generated is inherent to quantum mechanics, making quantum systems a perfect source of entropy for random number generation [5]. Applications of QRNGs include those typical of random number generators such as Monte Carlo simulations, weather prediction, industrial testing, gambling, and quantitative finance. Specific applications of QRNGs can be found in fundamental-physics tests and particularly in quantum communications because use of these generators is a necessary security requirement for QKD [2].

Most existing QRNGs are based on quantum optics because of the availability of high-quality optical components and the possibility of chip-size integration [4]. Single-photon QRNGs [7–9] and multiphoton QRNGs [10–23] have been demonstrated. QRNGs based on gain-switching semiconductor lasers are an example of multiphoton QRNGs. They exploit the fact that the product of the interference of two pulses with random phases is a third pulse with random amplitude [2,16–23]. The advantages of QRNGs of these types include fast operation at rates of gigabits per second, robustness, low cost, operation with flexible clock frequencies, use of standard photodetectors due to the high signal level, and full integration on an InP platform [22]. In these generators the current applied to a single-mode laser diode is periodically modulated from a well-below-threshold value to a value

*valle@ifca.unican.es

above the threshold to obtaining gain-switching operation [13,16–18,21–23]. While the laser is operated below the threshold, the evolution of the optical phase becomes random due to the spontaneous-emission noise. The laser emits then a series of pulses with a random phase. Phase fluctuations are converted into amplitude fluctuations by use of an unbalanced Mach-Zehnder interferometer, with a delay matching the pulse repetition period. Detection and postprocessing of the amplitude values provide the generation of random numbers. Fast generation rates (quantum random bit generation of up to 43 Gbit/s) have been shown experimentally [16].

The above-mentioned generators belong to the class of trusted-device QRNGs [4]. In these systems it is very useful to build a model of the physical entropy source to guarantee unpredictability, in the sense that the device is generating randomness of genuine quantum origin [23]. By use of numerical simulations of the stochastic rate equations that quantify the phase noise, a comparison with the experimental results is performed to validate the operational limits of the phase-noise QRNG [23]. This validation process can be used to check the device performance to detect malfunctioning or malicious manipulation of the QRNG [23]. A good quantitative description of experimental phase noise using stochastic-rate-equation modeling can be obtained only when extraction of the parameters of the semiconductor laser is performed [23,24].

Experimental and theoretical studies of laser-light fluctuations began in the late 1960s [25–29]. Study of fluctuations of the light emitted by semiconductor lasers has also received much attention [30–37]. A theoretical description, deduced from first principles and valid for below-threshold and above-threshold operation, has been provided that is based on the Fokker-Planck equation or alternatively on stochastic rate equations of the Langevin type [27,38]. The dynamical description of the statistics of the optical phase in gain-switched semiconductor lasers, which are the basis of phase-noise QRNGs, was performed using these Langevin equations [2,16,19,21,23,24,39,40], which correspond to the widely used models described in Refs. [30, 31,33,34]. Quantifying the phase noise in gain-switched lasers is also important in the context of QKD, where phase randomization is essential to security [2,23,41].

Most of the previous stochastic rate equations consider the evolution for the carrier and photon densities inside the device and the optical phase of the laser [2,16,19, 21,23,39]. Numerical integration of these equations using explicit methods such as the first-order Euler-Maruyama method or the second-order Milstein method or implicit methods such as Heun's predictor-corrector algorithm present numerical instabilities when the laser is below the threshold [40], which is precisely the regime in which most of the phase randomization occurs. When the photon number is very small, random fluctuations that model the spontaneous-emission noise can produce a negative value of the photon number. Numerical instabilities appear because the photon number appears inside the square-root factors that multiply the noise terms in the equations for the photon number and optical phase. These instabilities can be avoided when the corresponding rate equations for the laser electric field and carrier number are used [40].

In this work we use these electric field equations to analyze the phase statistics of the gain-switched laser. As mentioned above, their use avoids the previously described instabilities, but we show that a new problem appears: the variance of the optical phase becomes divergent. The divergence cannot be observed with the simulation of the equations for the photon number and optical phase because the appearance of the previous instabilities does not permit the correct calculation of the dynamical evolution when the power is very low. We find that the phase-variance divergence manifests itself as a monotonous increase of its value as the integration time step decreases. We compare the optical-phase evolution obtained with the stochastic rate equations with that obtained in two-dimensional Brownian motion. In this way, we use the long-known result of the divergence of the variance of the polar angle in the planar Brownian motion [42] to explain the divergence of the phase variance.

This paper is organized as follows. In Sec. II, we present our theoretical model. Section III is devoted to the presentation of the numerical results, with special emphasis on the divergence of the phase variance. In Sec. IV, we discuss the origin of this divergence. Finally, in Sec. V, we discuss and summarize the results.

II. THEORETICAL MODEL

The dynamics of a gain-switched single-mode laser diode can be modeled by use of a set of stochastic differential rate equations. These read (in Ito's sense) [2,16,19, 21,23,24,30,33,35,39,40,43]

$$\frac{dp}{dt} = \left[\frac{\Gamma v_g g(n)}{1+\bar{\epsilon}p} - \frac{1}{\tau_p}\right]p + \Gamma R_{\rm sp}(n) + \sqrt{2\Gamma R_{\rm sp}(n)p}F_p(t), \tag{1}$$

$$\frac{d\phi}{dt} = \frac{\alpha}{2}\left[\Gamma v_g g(n) - \frac{1}{\tau_p}\right] + \sqrt{\frac{\Gamma R_{\rm sp}(n)}{2p}}F_\phi(t), \tag{2}$$

$$\frac{dn}{dt} = \frac{I(t)}{eV_a} - R(n) - \frac{v_g g(n)p}{1+\bar{\epsilon}p}, \tag{3}$$

where $p(t)$ is the photon density, $\phi(t)$ is the optical phase in the reference frame corresponding to the resonant frequency at the threshold current [35], $n(t)$ is the carrier density, V_a is the active volume, e is the electron charge, v_g is the group velocity, $g(n)$ is the material gain, $\bar{\epsilon}$ is the nonlinear gain coefficient, Γ is the optical confinement factor, τ_p is the photon lifetime, α is the linewidth-enhancement

factor, $R(n)$ is the carrier recombination rate, and $R_{sp}(n)$ is the rate of the spontaneous emission coupled into the lasing mode. We consider a temporal dependence for the injected current, $I(t)$, and a material gain, $g(n)$, given by $g(n) = dg/dn(n - n_t)$, where dg/dn is the differential gain and n_t is the transparency carrier density. The Langevin terms $F_p(t)$ and $F_\phi(t)$ in Eqs. (1) and (2) represent fluctuations due to spontaneous emission, with the correlation property $< F_i(t)F_j(t') >= \delta_{ij}\delta(t - t')$, where $\delta(t)$ is the Dirac δ function and δ_{ij} the Kronecker δ function, with the subindices i and j referring to the variables p and ϕ. We do not take into account in our model the carrier noise terms because it has been shown that their effect on the statistics of the phase is very small in transient regimes [19,36,44].

We now write the corresponding equations for the number of photons inside the laser, $P(t)$, and the number of carriers in the active region, $N(t)$, by doing the following change of variables: $P = pV_p$ and $N = nV_a$, where V_p is the volume occupied by the photons. These equations read

$$\frac{dP}{dt} = \left[\frac{G_N(N - N_t)}{1 + \epsilon P} - \frac{1}{\tau_p}\right]P + \beta BN^2 + \sqrt{2\beta BP}NF_p(t), \tag{4}$$

$$\frac{d\phi}{dt} = \frac{\alpha}{2}\left[G_N(N - N_t) - \frac{1}{\tau_p}\right] + \sqrt{\frac{\beta B}{2P}}NF_\phi(t), \tag{5}$$

$$\frac{dN}{dt} = \frac{I(t)}{e} - (AN + BN^2 + CN^3) - \frac{G_N(N - N_t)P}{1 + \epsilon P}. \tag{6}$$

To obtain these equations, we considered that $R(n) = an + bn^2 + cn^3$ and $R_{sp}(n) = \beta bn^2$, where a, b, and c are the nonradiative-recombination, spontaneous-recombination, and Auger-recombination coefficients, respectively, and β is the fraction of spontaneous emission coupled into the lasing mode. The expressions for the new parameters are $G_N = \Gamma v_g dg/dn/V_a$, $N_t = n_t V_a$, $A = a$, $B = b/V_a$, $C = c/V_a^2$, and $\epsilon = \bar{\epsilon}\Gamma/V_a$. In deriving these equations, we also used that $\Gamma = V_a/V_p$.

When laser diodes are used for phase-noise QRNGs, a large signal modulation of $I(t)$ is considered in such a way that a random evolution of the phase is induced by the spontaneous-emission noise, specially when the bias current is below the threshold current, I_{th}. Information on the temporal dependence of the phase statistics under large-signal-current modulation has been obtained by numerical solution of Eqs. (1)–(3) [23,39] by use of the Euler-Maruyama method [27,45]. As discussed in the previous section, numerical integration of these equations is problematic: when P is very small, negative values of P can appear in the square-root factors that multiply the noise terms in Eqs. (4) and (5), causing instabilities. The usual solution for this problem is the integration of the corresponding rate equations for the complex electric field, E, instead of equations for p and ϕ [40,46]. These equations read [40]

$$\frac{dE}{dt} = \left[\left(\frac{1}{1 + \epsilon \mid E \mid^2} + i\alpha\right)G_N(N - N_t) - \frac{1 + i\alpha}{\tau_p}\right]\frac{E}{2} + \sqrt{\frac{\beta B}{2}}N\xi(t), \tag{7}$$

$$\frac{dN}{dt} = \frac{I(t)}{e} - (AN + BN^2 + CN^3) - \frac{G_N(N - N_t) \mid E \mid^2}{1 + \epsilon \mid E \mid^2}, \tag{8}$$

where $E(t) = E_1(t) + iE_2(t)$ is the complex electric field and $\xi(t) = \xi_1(t) + i\xi_2(t)$ is the complex Gaussian white noise with zero average and correlation given by $< \xi(t)\xi^*(t') >= 2\delta(t - t')$ that represents the spontaneous-emission noise. The application of the rules for the change of variables in Ito's calculus [38] to $P =\mid E \mid^2 = E_1^2 + E_2^2$ and $\phi = \arctan(E_2/E_1)$ in Eqs. (7) and (8) gives our initial equations (4)–(6), as explained in Appendix A. Integration of Eqs. (7) and (8) avoids the previously mentioned instabilities because P does not appear inside the square-root factors that multiply the noise terms, and hence no instabilities are observed. We include in Appendix B the equations corresponding to the implementation of the Euler-Maruyama method to our model. We also discuss in Appendix B the numerical procedure used to obtain the optical phase from the integration of the equations for the real and imaginary parts of the electric field.

III. NUMERICAL RESULTS

In this section we numerically solve Eqs. (7) and (8) by using the Euler-Maruyama algorithm [27,45]. We use the numerical values of the parameters that have been extracted for a discrete-mode edge-emitting laser [40,43]. This device is a single-longitudinal-mode semiconductor laser emitting close to a wavelength of 1550 nm and with $I_{th} = 14.14$ mA at 25 °C. The values of the parameters are as follows: $G_N = 1.48 \times 10^4$ s^{-1}, $N_t = 1.93 \times 10^7$, $\epsilon = 7.73 \times 10^{-8}$, $\tau_p = 2.17$ ps, $\alpha = 3$, $\beta = 5.3 \times 10^{-6}$, $A = 2.8 \times 10^8$ s^{-1}, $B = 9.8$ s^{-1}, and $C = 3.84 \times 10^{-7}$ s^{-1} [40,43]. Simulation and experimental results have shown not only qualitative agreement but also a remarkable quantitative agreement for a very wide range of gain-switching conditions [24,40,43,47].

We consider an injected bias current that follows a square-wave modulation of period T with $I(t) = I_{on}$ during $T/2$ and $I(t) = I_{off}$ during the rest of the period. We take the following values: $I_{on} = 30$ mA and $T = 1$ ns. The laser is switched off with I_{off} below the threshold value to get randomness of the phase due to the spontaneous-emission noise. The temporal evolution during several consecutive periods of P, N, and ϕ when $I_{off} = 7$ mA is plotted in Fig. 1 in Ref. [44]. Similar evolutions but plotted in one time window of duration T can be found in Fig. 5 in Ref. [40]. In

that figure, the initial conditions for one period correspond to the final values of the variables at the end of the previous period. The final value of the phase at the end of the period, $\phi(T)$, leaves the $[0, 2\pi)$ interval, so the initial value of the phase, $\phi(0)$, must be converted to the $[0, 2\pi)$ range if we want to obtain well-defined statistical moments of ϕ [40,44]. This is done by taking $\phi(0)$ as $\phi(0) = \phi(T) - \text{int}\big(\phi(T)/2\pi\big)2\pi$ [40,44].

Figures 1(a)–1(c) show the dynamical evolution of the averaged photon number, carrier number, and optical phase, respectively. The values of the rate-equation parameters and the integration time step (0.01 ps) are similar to the values used in Ref. [40]. The effect of spontaneous-emission noise on some individual realizations under the same modulation conditions as for Fig. 1 is well illustrated in Fig. 5 in Ref. [40] with its corresponding discussion. Fluctuations of P and ϕ are more important at the beginning and at the end of the period (before 0.1 ns and after 0.7 ns, respectively). Since P is small in those regions, the noise terms dominate in Eqs. (4) and (5) [40]. Figure 1(d) shows the dynamical evolution of the standard deviation of the phase, σ_ϕ, which is the relevant quantity for determining the performance of the gain-switched laser diode as a QRNG. The initial value is larger than zero due to our choice of random initial conditions. The two large increases of $\sigma_\phi(t)$ occur at the beginning and at the end of the period and correspond to a phase-diffusion regime because in those regions P has small values determined by the spontaneous-emission noise.

Figure 2 shows the effect of decreasing the integration time step, Δt, on the dynamical evolution of the phase statistics. A change of several orders of magnitude, from $\Delta t = 10^{-1}$ ps to $\Delta t = 10^{-6}$ ps, is considered. Figure 2(a) shows that the averaged phase quickly achieves convergent values because it does not change significantly with Δt. A similar convergence (not shown) occurs with the averaged values and standard deviations of P and N. However, the behavior of the variance of the optical phase, $\sigma_\phi^2(t)$, is radically different, as shown in Fig. 2(b). There is no evidence of the convergence of this quantity as the time step is decreased, even for values of Δt as small as 10^{-5} or 10^{-6} ps. The differences between results for different time steps appear at the beginning and at the end of the period. In these regions, linear increases of $\sigma_\phi^2(t)$ with t appear with slopes that increase as Δt is decreased. The linear increase of the phase variance is characteristic of the phase-diffusion process. The fact that the slope of $\sigma_\phi^2(t)$ in the phase-diffusion regime keeps on increasing when Δt decreases indicates that the phase variance is a divergent quantity: its value can be arbitrarily large providing that a small-enough integration time step is considered.

To show that there is no sign of convergence in the values of the previous slopes, and in consequence of the phase-variance values, we calculate the slope of σ_ϕ^2 versus t at the beginning and at the end of the period. The results

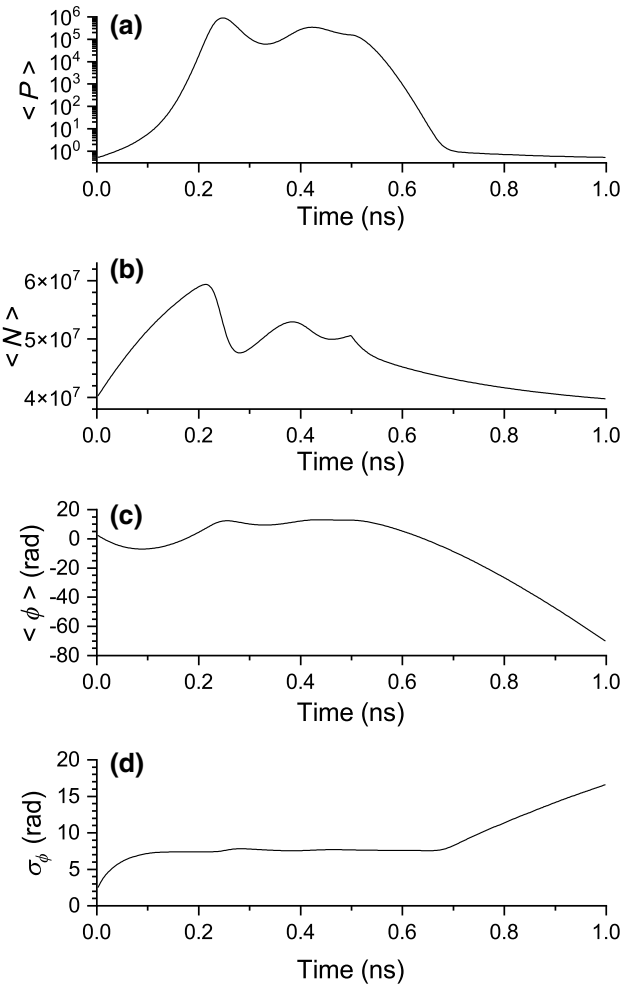

FIG. 1. (a) Averaged photon number, (b) averaged carrier number, (c) averaged phase, and (d) standard deviation of the phase as a function of time. $I_{\text{off}} = 7$ mA, the number of periods is 5×10^4, and the integration time step is 0.01 ps.

are shown in Fig. 3 for the different Δt values considered in Fig. 2. The initial (final) slope is calculated by linear fitting of the values included in Fig. 2 from 0 to 0.025 ns (from 0.9 to 1 ns). Adjusted R^2 merit values, $\bar{R}^2$, which give information on the goodness of the fit, range from 0.99850 to 0.99992, indicating that good linear fits are obtained.

The fact that phase diffusion is the dominant process at the beginning and at the end of the period should result in similar slopes in those time regions. Figure 3 shows that the values of the initial and final slopes are similar. More importantly, Fig. 3 also shows that both slopes increase as the time step decreases, with no sign of saturation at the smallest values of Δt. The plot in Fig. 3 has a logarithmic horizontal axis. Figure 3 also shows that the slope depends linearly on $\ln \Delta t$, so the phase divergence is characterized by a logarithmic dependence of the slope on Δt: the slope is equal to $-c_1 \ln \Delta t + c_2$, where

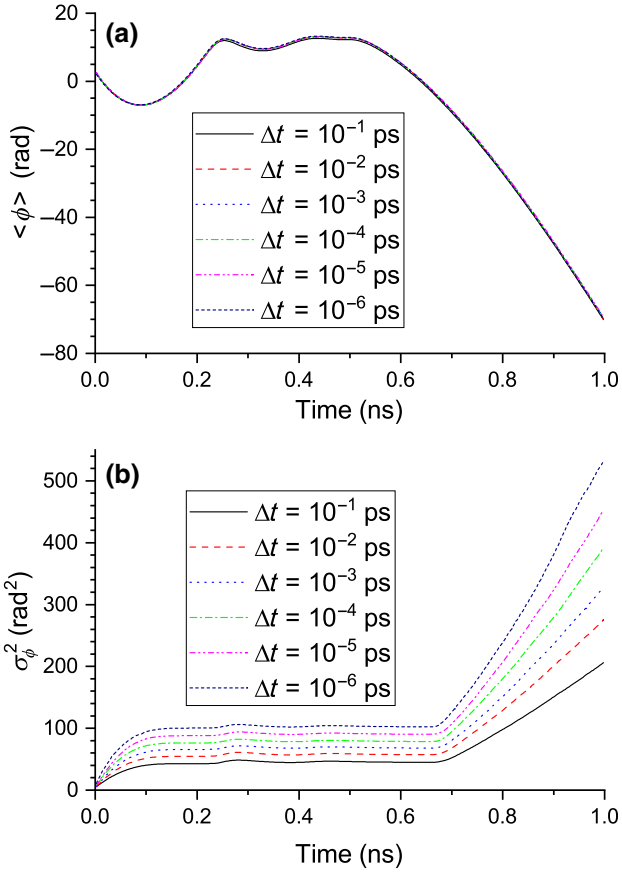

FIG. 2. (a) Averaged phase and (b) variance of the phase as a function of time. Results for different integration time steps are plotted with lines of different colors, as indicated in the insets. $I_{\text{off}} = 7$ mA and the number of periods is 5×10^4.

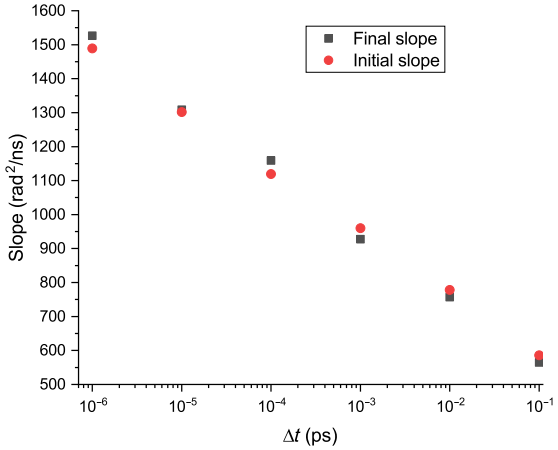

FIG. 3. (a) Slope of the phase variance versus time as a function of the integration time step. Results for the final and initial parts of the period are plotted with different symbols.

$c_1, c_2 > 0$. Linear fitting of the data in Fig. 3 gives an initial slope of $-77.525 \ln \Delta t + 414.277$, $\bar{R}^2 = 0.9993$, and a final slope of $-83.062 \ln \Delta t + 371.362$, $\bar{R}^2 = 0.9976$. The divergence of the phase variance is then characterized by the previous logarithmic dependence because if we calculate the change of σ_ϕ^2 during a time interval (t_1, t_2) in which phase diffusion dominates the evolution, we obtain $\sigma_\phi^2(t_2) - \sigma_\phi^2(t_1) = (-c_1 \ln \Delta t + c_2)(t_2 - t_1)$.

IV. EXPLAINING THE DIVERGENCE

We explain the divergence of the phase by using the analogy of our problem, under certain restrictions, to the simplest two-dimensional Brownian motion, which corresponds to a particle diffusing in a plane subjected only to a random force. We first consider a semiconductor laser biased slightly below the threshold, $I_{\text{off}} \lesssim I_{\text{th}}$, and with $\alpha = 0$. In this case, $E/2$ and the term that multiplies it in Eq. (7) are small and the noise term dominates the evolution at the beginning and at the end of the period. In this way, we can approximate Eq. (7) by

$$\frac{dE}{dt} = \sqrt{\frac{\beta B}{2}} N \xi(t). \tag{9}$$

Since the real and imaginary parts of $\xi(t)$, $\xi_1(t)$ and $\xi_2(t)$, are independent Gaussian white noise, the evolution of the real and imaginary parts of the electric field, $E_1(t)$ and $E_2(t)$, is described by two-dimensional Brownian motion. $E_1(t)$ and $E_2(t)$ are independent Gaussian processes, each with zero mean value and diffusing with a diffusion coefficient given by $\beta B N^2/2$. We also note that considering $\alpha = 0$ means that the phase evolution is affected only by the spontaneous-emission-noise term, as can be seen in Eq. (5).

A first clue to the divergent behavior of the phase is given by the distribution of the ratio of those two Gaussians, E_2/E_1, since its calculation is an intermediate step to calculate the phase. It is shown in Ref. [48] that the probability density of this ratio is that corresponding to a Cauchy distribution, which is a well-known example of a continuous random variable with infinite variance. However, the quantity of interest is the phase, $\phi = \arctan(E_2/E_1)$, so we extend our discussion using the well-established mathematical theory of two-dimensional Brownian motion.

A freely diffusing particle in two dimensions (i.e., one executing two-dimensional Brownian motion) can be described mathematically in polar coordinates. Since $E_1(t)$ and $E_2(t)$ are continuous stochastic processes, the polar angle, $\phi(t)$, of the corresponding planar Brownian motion has the freedom to vary from $-\infty$ to ∞. $\phi(t)$ is the winding number of the continuous path $E(\tau) = E_1(\tau) + iE_2(\tau)$, $0 \le \tau \le t$, about the origin [49]. $\phi(t)$ is a continuous function of t with probability 1 (the probability is zero that $E(t)$=0 in any t interval) [42,49]. Since ϕ takes values in $(-\infty, \infty)$ instead of $[0, 2\pi)$, we can view the planar

Brownian motion as occurring in the universal cover of $\mathbb{C} \setminus \{0\}$, which is the Riemann surface of $\ln z$. There is a long-known but particularly striking feature of polar-angle evolution in the planar Brownian motion: $\phi(t)$ has infinite variance, $\sigma_\phi^2(t) = \infty$, as Lèvy demonstrated [42] from the fact that $\phi(t)$ tends to assume very large values due to the roughness of the Brownian trajectory when $P(t)$ is close to zero. This arises from the fractal nature, the infinitesimal, infinitely frequent, random-walk steps of the planar Brownian motion, and applies whatever the starting radius, $\sqrt{P(0)}$, is from the origin [50].

The reason why we observe the divergence described in the previous section is the infinite value of the variance of the phase. We show in Fig. 4 the evolution of $P(t)$ and $\phi(t)$ for different random trajectories when $\alpha = 0$ and $I_{\text{off}} = 0.9I_{\text{th}}$ (12.73 mA). Results obtained with $\Delta t = 10^{-1}$ ps and $\Delta t = 10^{-5}$ ps are shown in Figs. 4(a) and 4(c) and Figs. 4(b) and 4(d), respectively. In each plot we show five typical trajectories and a nontypical trajectory (solid black line) for which the maximum value of $|\phi(t)|$ us obtained in a simulation with 5×10^4 periods. It is clear in Figs. 4(a) and 4(b) how the spontaneous-emission noise dominates the evolution at the beginning and at the end of the period. Figures 4(c) and 4(d) shows that the realizations of ϕ are continuous functions of t in such a way that they are also dominated by noise in the previously mentioned regions. It is clear from Figs. 4(a) and 4(c) that the largest excursions of the phase appear in the trajectories that get closer to zero (see the evolution of the solid black lines close to 0.82, 0.85, and 0.91 ns). In these cases there are more rotations induced by the noise around the origin of the complex plane (E_1, E_2). Figures 4(b) and 4(d) show the results obtained when Δt has decreased by 4 orders of magnitude. The decrease of Δt results in more-frequent rotations induced by noise around the origin for a given trajectory. This can be seen by comparing the two trajectories with the largest phase excursions in Figs. 4(c) and 4(d): these excursions widen when Δt decreases. The maximum value of the phase, $\phi/2\pi$, observed for our simulations with 5×10^4 trajectories is 6.63, 10.44, 11.22, 12.03, and 12.97 for $\Delta t = 10^{-1}, 10^{-2}, 10^{-3}, 10^{-4}$, and 10^{-5} ps, respectively.

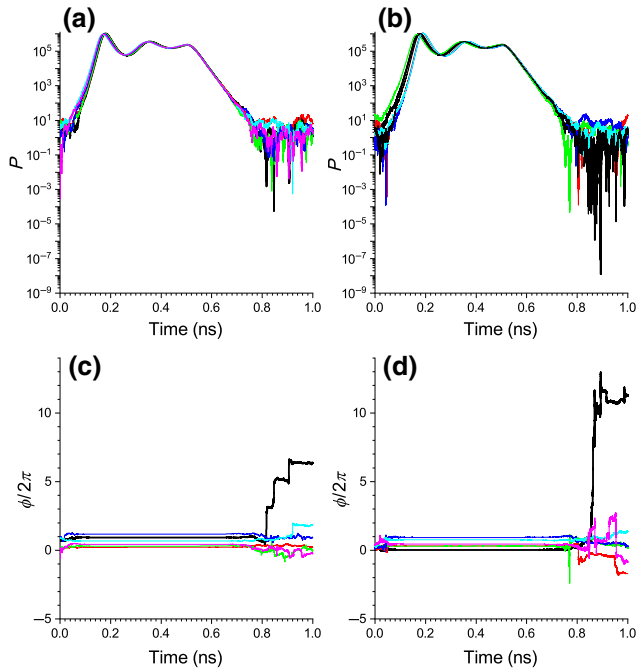

FIG. 4. Different realizations of the (a),(b) photon number and (c),(d) optical phase as a function of time. The integration time step is 10^{-1} ps in (a),(c) and 10^{-5} ps in (b),(d). $\alpha = 0$ and $I_{\text{off}} = 12.73$ mA. The trajectory for which the maximum value of $|\phi(t)|$ is obtained in a simulation with 5×10^4 periods is plotted with a solid black line.

Widening of the random trajectories as Δt decreases was previously discussed with those in which the excursions are maxima but also occurs for the other trajectories. Since the averaged phase and variance are calculated with use of a fixed number of trajectories, the previous widening results in an increase of the variance of the phase in the diffusing regions as Δt decreases, as can be seen in Fig. 5. These increases are similar to those shown in Fig. 2(b). The discussion using the visualization of random trajectories is done for the case of $\alpha = 0$ and $I_{\text{off}} = 0.9I_{\text{th}}$ because the effects of drift in the phase are minimized in such a way that we have a better correspondence with the two-dimensional free Brownian motion.

We now discuss the situation found when we have a realistic value of α and a smaller value of I_{off} so as to have a stronger effect of the phase diffusion ($\alpha = 3$, $I_{\text{off}} = 7$ mA), which is the precisely the case described in the previous

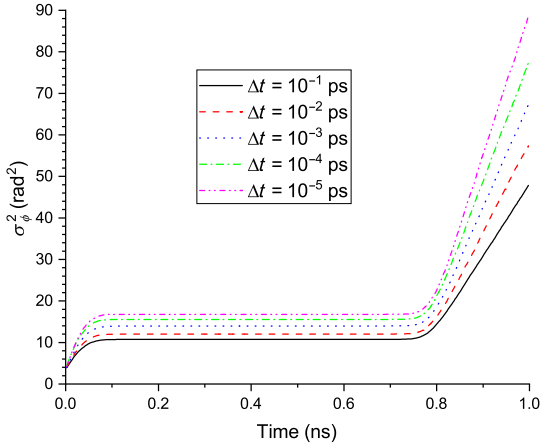

FIG. 5. Variance of the phase as a function of time. Results for different integration time steps are plotted with lines of different colors, as indicated in the inset. $\alpha = 0$, $I_{\text{off}} = 12.73$ mA, and the number of periods is 5×10^4.

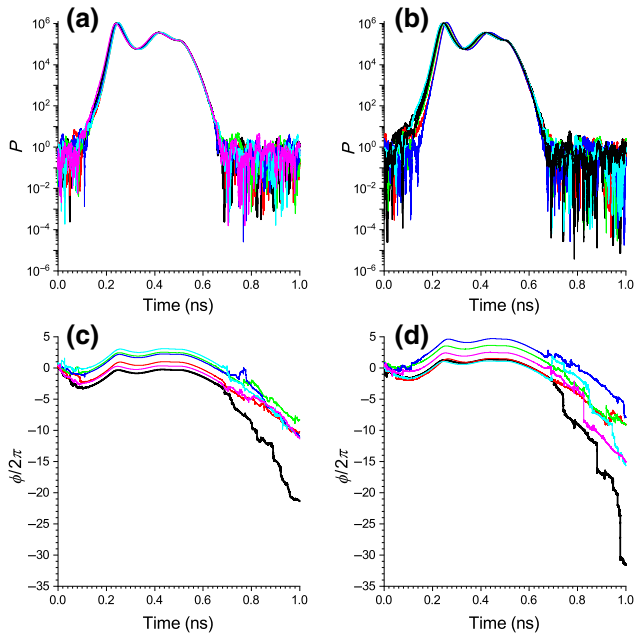

FIG. 6. Different realizations of the (a),(b) photon number and (c),(d) optical phase as a function of time. The integration time step is 10^{-1} ps in (a),(c) and 10^{-5} ps in (b),(d). $\alpha = 3$ and $I_{\text{off}} = 7$ mA. The trajectory for which the maximum value of $|\,\phi(t)\,|$ is obtained in a simulation with 5×10^4 periods is plotted with a solid black line.

section. Figure 6 shows $P(t)$ and $\phi(t)$ for six different random trajectories obtained with two different values of Δt (10^{-1} and 10^{-5} ps).

Again we show the trajectory for which the maximum value of $|\,\phi(t)\,|$ is obtained in our simulations and the trajectories corresponding to five consecutive periods. Figures 6(c) and 6(d) show that both deterministic drift and fluctuations of the phase are important in determining the value of the phase at the beginning and at the end of the period. While P is large, the phase evolution is mainly deterministic, being characterized by the relaxation oscillations before $t = T/2$ and a monotonous decrease after $t = T/2$ since $N(t) < N_{\text{th}}$ [see Eq. (5)]. Figure 6 shows that the largest excursions of the phase appear in the trajectories that get closer to zero [see, for instance, the evolution of the solid black lines close to 0.74, 0.88, and 0.98 ns in Figs. 6(b) and 6(d)]. Also, comparison between Figs. 6(a) and 6(b) shows that when Δt decreases, the minimum values of P are closer to zero, with more-frequent rotations induced by noise around the origin of the complex plane. This is seen by the widening of the trajectory with the largest phase excursions in Figs. 6(c) and 6(d) as Δt decreases. Widening of typical random trajectories as Δt decreases is clearly seen when we compare Figs. 6(c) and 6(d). Widening of trajectories explains the increase of the variance of the phase in the diffusing regions as Δt decreases, as shown in Fig. 2(b).

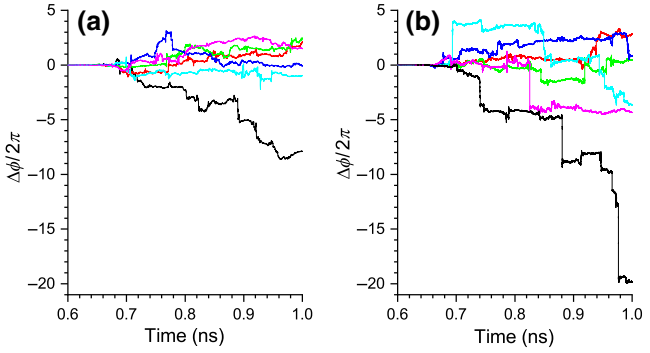

FIG. 7. Difference between the random phase of the trajectories in Fig. 6 and their corresponding deterministic phase. Each trajectory is identified with the same color in Fig. 6 and here. The plots in (a),(b) correspond to Figs. 6(c) and 6(d), respectively.

We show in Fig. 7 the difference between the random phase of the trajectories in Fig. 6, $\phi(t)$, and their corresponding deterministic phase, $\phi_{\text{det}}(t)$; that is, $\Delta\phi(t) = \phi(t) - \phi_{\text{det}}(t)$. The values of $\phi_{\text{det}}(t)$ are calculated from the integration of the deterministic rate equations from the initial conditions at $t = 0.2$ ns, a time at which a deterministic evolution has been reached for all the trajectories. Under these conditions the effect of noise becomes important just before $t = 0.7$ ns and the features discussed for Fig. 6 are better visualized: the large random excursions of the phase at 0.74, 0.88, and 0.98 ns are well seen in Fig. 7(b), and the increasing widening of trajectories as the integration step decreases is also well seen by comparison of Figs. 7(a) and 7(b).

Another way of understanding the divergence of the variance of the phase is by using the following result. Spitzer [49] showed that the normalized winding angle obtained with unit diffusivity, $\Theta(t)$, converges to a standard Cauchy distribution as $t \to \infty$:

$$\frac{2\Theta(t)}{\ln t} \xrightarrow{d} X, \quad f(x) = \frac{1}{\pi}\frac{1}{1+x^2}, \tag{10}$$

where $f(x)$ is the probability density of X. This means that given a large t, $\Theta(t)$ and so $\phi(t)$ behave as a Cauchy distribution, having therefore an infinite variance. This divergence can be numerically manifested when one simulates X by using the method of the cumulative distribution function, $F_X(x)$. For the normalized Cauchy distribution, $F_X(x) = 1/2 + \arctan(x)/\pi$, for $-\infty < x < \infty$. Values of X are numerically obtained by use of $x = F_X^{-1}(u) = \tan(\pi(u - 1/2))$, where u, $0 < u < 1$, is distributed according the uniform random variable, $U(0, 1)$. As the number of simulated values of u increases, values closer to 0 and 1 are obtained that result in values of x closer to $-\infty$ and ∞, respectively. The role of these numbers in determining numerically the average of X^2,

$< X^2 >$, is essential because $< X^2 >$ keeps on increasing as the number of simulated x values is increased.

We complete the discussion on the divergence of the phase variance by including in Appendix C a calculation of this quantity when the system reaches the steady state for a current below the threshold value. We find that σ_ϕ^2 is proportional to $< 1/P >$, which is a divergent quantity because P is an exponential random variable for the below-threshold operation.

V. DISCUSSION AND SUMMARY

The numerical integration of Eqs. (4)–(6) presents numerical instabilities as mentioned earlier. In the simulations of these equations using the Euler-Maruyama scheme, the unphysical results due to negative values of P and N have been treated by solving the equations with the constraint that P and N are non-negative [39]. However no details are given in Ref. [39] for how that constraint is implemented. In that work, simulations were performed at different integration steps such that $\Delta t < 0.1$ ps in such a way that the results obtained at different Δt values were the same for all simulations [39]. Therefore when that scheme is used, there is a convergence, but not to the correct mathematical solution of Eqs. (4)–(6) because as we show in this work, no convergence is achieved when we solve the equivalent field equations that avoid the numerical instabilities. The main reason for this difference is that the integration of Eqs. (7) and (8) describes well the evolution close to $P = 0$ given by stochastic-rate-equation modeling. The fact that there are several mathematical theorems [42,49] confirming the divergence of the polar angle in two-dimensional Brownian motion gives us confidence in our results.

A correct numerical integration in the below-threshold regime is essential when one is describing QRNGs and QKDs based on gain-switching laser diodes because that is precisely the regime where phase randomization mainly occurs [23,41]. As we show, integration using stochastic rate equations for the photon number and phase does not describe well the phase statistics below the threshold. Simulations must be performed using the equations for the complex field, from which we obtain the values of P and ϕ at each integration step. However, our results show that the phase variance is a divergent quantity, with a value that increases as the integration step is decreased. This divergence is slow but it is still a divergence, meaning that we cannot obtain a well-defined value of the phase variance when using stochastic rate equations in the below-threshold regime. In this way, stochastic rate equations for $P(t)$ and $\phi(t)$ [2,23,39,40,51] or for complex $E(t)$ [40] cannot describe well the experimental phase statistics when the photon number is small.

The main reason for this result lies in the idealized mathematical formulation of the spontaneous-emission noise as white noise, $\xi(t)$, which is a quantity with no correlation at different times and with the rather pathological result that $\xi(t)$ has infinite variance [38]. We find that the use of white noise as an idealization of a realistic fluctuating signal causes problems when one is describing some variables of the system, the optical phase in our case.

A possible solution of this problem could be modeling the spontaneous-emission noise with a realistic version of almost-uncorrelated noise, for instance, an Ornstein-Uhlenbeck process with a very small value of the correlation time. We do not know the order of magnitude of that correlation time, but it could be established by comparing experimental measurements of the phase variance, such as those reported in Ref. [23,39], with the numerical predictions of the stochastic rate equations for $E(t)$ driven by colored noise, instead of white noise. We would expect a convergent behavior of the phase variance at integration time steps determined by the correlation time of the noise.

A rigorous treatment of spontaneous emission would require quantization of the electric field. At the most-fundamental level, the origin of these fluctuations (intensity and phase fluctuations) lies in the quantum nature of the lasing process itself [31]. A proper description requires a quantum mechanical formulation of the rate equations using quantum Langevin terms [25,52] or master equations [52]. Stochastic rate equation models (SREMs) such as those used in this work are approximations that worsen as the photon number decreases. There are two types of SREM. The first one, SREM1, corresponds to that derived from first principles by Lax and Louisell [26] and Henry [34] for a system where the matter and radiation have reached equilibrium. In the derivation, a constant bias current is assumed in such a way that the steady-state average values of the variables appear in the terms that multiply $F_p(t)$ and $F_\phi(t)$ in Eqs. (4) and (5) [see Eqs. (19) and (20) in Ref. [24] for comparison]. Both types of noise appear as additive noise in SREM1. With use of this model, when the steady state corresponding to a bias current below the threshold has been reached, the optical phase diffuses with a variance that increases linearly with time. No divergence of the phase variance is observed because the phase evolution is analogous to one-dimensional Brownian motion.

The situation is different when we are considering a high-frequency modulation of the bias current. The laser is in a transient regime, the matter-radiation equilibrium has not been achieved yet, and the exact form of the spontaneous-emission noise terms is unknown [37]. A second type of model, SREM2, is considered in which the steady-state averaged values of the variables in the noise terms are replaced by the corresponding variables so as to analyze transient situations. This approximation is the one considered in this work [corresponding to Eqs. (4) and (5) or to Eq. (7)], and is commonly used in the analysis of phase-noise QRNGs [2,16,19,21,23,24,39,40]. To the best

of our knowledge, this approximation has not been justified in a rigorous way. The use of this approximation has been successful in describing the experimental results relative to the statistics in transient regimes of quantities related to the laser power, such as the turn-on timing jitter. However, our work shows that this approximation fails when we analyze the statistics of the optical phase. In this approximation, spontaneous-emission fluctuations appear as multiplicative noise in SREM2, the phase evolution is analogous to that found in two-dimensional Brownian motion, and the divergence of the phase variance is observed. These results also hold for a constant bias current when SREM2 is used, so an analysis of phase fluctuations using SREM1 is more appropriate. This analysis was performed in Ref. [24], in which a good comparison between experimental and theoretical phase variance was obtained when the current is larger than 0.6 times the threshold current. For smaller values of the current, the theoretical results clearly underestimate the experimental values, so a theoretical model better than SREM1 is needed to describe the phase fluctuations.

Another consequence of our results is related to the recently proposed procedure for finding the operational limits of a phase-noise QRNG [23]. This method is based on quantifying numerically and experimentally the amount of phase-noise randomness produced by a gain-switched laser diode. In the method, the intensity distribution at the output of the interferometer of the QRNG is measured. An experimental value of the phase variance is extracted from a fit to the previous intensity distribution. A successful comparison of this value with the Monte Carlo simulation results is needed to validate the operational limits of the QRNG. Since the results of those simulations depend on the integration time step, the results of that comparison will depend on that step. To obtain a better method for comparison, we propose a slight modification of the process. This consists in using the full width at half maximum (FWHM) of the phase distribution in the validation method instead of the values of the phase variance. We have shown that the phase converges to a standard Cauchy distribution. This random variable has infinite variance but finite FWHM. Calculation of FWHM would avoid the dependence on the integration time step of the quantities used in the validation method.

In summary, we analyze theoretically the phase diffusion in a gain-switched single-mode semiconductor laser. By using simulations of the stochastic rate equations for the electric field, we show that the variance of the optical phase is a divergent quantity. This result can be explained by use of the analogy with the mathematical description of two-dimensional Brownian motion, for which it was shown that the variance of the polar angle is infinite [42]. The fact that this divergence is not observed with the simulation of the photon-number and phase equations [39] indicates that usual simulations of that model are not suitable for describing the phase statistics when the photon number is small: the results of the simulation converge, but not to the correct mathematical solution. Simulation of the stochastic rate equations for the electric field is better because they are consistent with the mathematical results but they still have the problem of giving rise to unphysical results since an infinite value is obtained for the phase variance, a quantity that can be experimentally obtained [23,39]. Our results show that stochastic-rate-equation models are not appropriated for describing the phase statistics when the photon number is small. A more-fundamental theoretical description of spontaneous emission is desirable to better characterize the experimental phase statistics in that regime. Our work has impact on quantum random number generation and QKD based on gain-switching of laser diodes where phase randomization, with its corresponding good theoretical description, is essential to security.

ACKNOWLEDGMENTS

The author acknowledges financial support from the Ministerio de Ciencia e Innovación (MCIN), Spain (Grant No. PID2021-123459OB-C22, MCIN/AEI/10.13039/501100011033/FEDER, UE). The author is also grateful to Miguel Angel Rodriguez for useful comments.

APPENDIX A: EQUIVALENCE BETWEEN RATE-EQUATION MODELS

Here we use the Ito calculus to derive Eqs. (4) and (5) from the rate equation for the complex electric field. We first separate Eq. (7) into the equations for the real and imaginary parts of $E(t)$, $E_1(t)$ and $E_2(t)$, to obtain

$$\frac{dE_1}{dt} = A_1 + \sqrt{\frac{\beta B}{2}} N \xi_1(t), \tag{A1}$$

$$\frac{dE_2}{dt} = A_2 + \sqrt{\frac{\beta B}{2}} N \xi_2(t), \tag{A2}$$

where

$$A_1 = \left(\frac{G_N(N - N_t)}{1 + \epsilon \mid E \mid^2} - \frac{1}{\tau_p} \right) \frac{E_1}{2} - \alpha \left(G_N(N - N_t) - \frac{1}{\tau_p} \right) \frac{E_2}{2}, \tag{A3}$$

$$A_2 = \left(\frac{G_N(N - N_t)}{1 + \epsilon \mid E \mid^2} - \frac{1}{\tau_p} \right) \frac{E_2}{2} + \alpha \left(G_N(N - N_t) - \frac{1}{\tau_p} \right) \frac{E_1}{2}, \tag{A4}$$

and ξ_1 and ξ_2 are real independent Gaussian noise with $< \xi_i(t) >= 0$ and $< \xi_i(t)\xi_j(t') >= \delta_{ij}\delta(t - t')$, $i,j = 1,2$.

The change of variables is performed by use of Ito's formula [38]. Given an n-dimensional vector $\mathbf{x}(\mathbf{t})$ satisfying

the stochastic differential equation

$$d\mathbf{x} = \mathbf{A}(\mathbf{x},t) + \mathbb{B}(\mathbf{x},t)d\mathbf{W}(t), \tag{A5}$$

where $d\mathbf{W}(t)$ is an n-dimensional vector formed by n independent differential Wiener processes, a function of $\mathbf{x}$, $f(\mathbf{x})$, satisfies [38]

$$\begin{aligned} df(\mathbf{x}) = &\sum_i A_i(\mathbf{x},t)\partial_i f(\mathbf{x})dt \\ &+ \frac{1}{2}\sum_{i,j}\left[\mathbb{B}(\mathbf{x},t)\mathbb{B}^T(\mathbf{x},t)\right]_{ij}\partial_i\partial_j f(\mathbf{x})dt \\ &+ \sum_{i,j}\mathbb{B}_{ij}(\mathbf{x},t)\partial_i f(\mathbf{x})dW_j(t). \end{aligned} \tag{A6}$$

In our two-dimensional case, $\mathbf{x} = \begin{bmatrix} E_1 \\ E_2 \end{bmatrix}$, $\mathbf{A} = \begin{bmatrix} A_1 \\ A_2 \end{bmatrix}$, and $d\mathbf{W} = \begin{bmatrix} dW_1 \\ dW_2 \end{bmatrix}$. The elements of the $\mathbb{B}$ matrix are $\mathbb{B}_{11} = \mathbb{B}_{22} = \sqrt{\beta B/2}N$, $\mathbb{B}_{12} = \mathbb{B}_{21} = 0$, and $dW_i = \xi_i(t)dt$. Application of Eq. (A6) to $f(\mathbf{x}) = E_1^2 + E_2^2 = P$ gives

$$\begin{aligned} dP = &\left[\left(\frac{G_N(N-N_t)}{1+\epsilon\mid E\mid^2} - \frac{1}{\tau_p}\right)P + \beta BN^2\right]dt \\ &+ \sqrt{2\beta B}N(E_1dW_1 + E_2dW_2). \end{aligned} \tag{A7}$$

Taking into account that $E_1(t) = \sqrt{P(t)}\cos\phi(t)$ and $E_2(t) = \sqrt{P(t)}\sin\phi(t)$, and defining

$$dW_p(t) = dW_1(t)\cos\phi(t) + dW_2(t)\sin\phi(t), \tag{A8}$$

$$dW_\phi(t) = -dW_1(t)\sin\phi(t) + dW_2(t)\cos\phi(t), \tag{A9}$$

we obtain

$$\begin{aligned} dP = &\left[\left(\frac{G_N(N-N_t)}{1+\epsilon P} - \frac{1}{\tau_p}\right)P + \beta BN^2\right]dt \\ &+ \sqrt{2\beta BP}NdW_p(t). \end{aligned} \tag{A10}$$

Equations (A8) and (A9) correspond to an orthogonal transformation in which $dW_p(t)$ and $dW_\phi(t)$ are increments of independent Wiener processes $W_p(t)$ and $W_\phi(t)$ [38]. In this way, $dW_p(t) = F_p(t)dt$ and $dW_\phi(t) = F_\phi(t)dt$, where $< F_p(t) >=< F_\phi(t) >= 0$, $< F_p(t)F_p(t') >=< F_\phi(t)F_\phi(t') >= \delta(t-t')$, and $< F_p(t)F_\phi(t') >= 0$. Equation (A10) is equivalent to Eq. (4), so the derivation of Eq. (5) still remains. This is done by application of Eq. (A6) to $f(\mathbf{x}) = \arctan(E_2/E_1) = \phi$:

$$\begin{aligned} d\phi = &\frac{1}{P}\left[-A_1E_2 + A_2E_1\right]dt \\ &+ \sqrt{\frac{\beta B}{2}}\frac{N}{P}(-E_2dW_1 + E_1dW_2). \end{aligned} \tag{A11}$$

Applying Eqs. (A3) and (A4), $E_1 = \sqrt{P}\cos\phi$, $E_2 = \sqrt{P}\sin\phi$, and Eq. (A9), we obtain

$$d\phi = \frac{\alpha}{2}\left[G_N(N-N_t) - \frac{1}{\tau_p}\right]dt + \sqrt{\frac{\beta B}{2P}}NdW_\phi, \tag{A12}$$

which is the same as Eq. (5)

APPENDIX B: NUMERICAL INTEGRATION OF THE FIELD EQUATIONS

The Euler-Maruyama algorithm corresponding to Eqs. (7) and (8) can be obtained after Eq. (7) has been split into equations for the real and imaginary parts of $E(t)$. The numerical algorithm reads

$$\begin{aligned} E_1(t+\Delta t) = &E_1(t) + \left(\frac{G_N(N(t)-N_t)}{1+\epsilon(E_1^2+E_2^2)(t)} - \frac{1}{\tau_p}\right)\frac{E_1(t)}{2}\Delta t \\ &- \alpha\left(G_N(N(t)-N_t) - \frac{1}{\tau_p}\right)\frac{E_2(t)}{2}\Delta t \\ &+ \sqrt{\frac{\beta B\Delta t}{2}}N(t)X_1, \end{aligned} \tag{B1}$$

$$\begin{aligned} E_2(t+\Delta t) = &E_2(t) + \left(\frac{G_N(N(t)-N_t)}{1+\epsilon(E_1^2+E_2^2)(t)} - \frac{1}{\tau_p}\right)\frac{E_2(t)}{2}\Delta t \\ &+ \alpha\left(G_N(N(t)-N_t) - \frac{1}{\tau_p}\right)\frac{E_1(t)}{2}\Delta t \\ &+ \sqrt{\frac{\beta B\Delta t}{2}}N(t)X_2, \end{aligned} \tag{B2}$$

$$\begin{aligned} N(t+\Delta t) = &N(t) + \frac{I(t)}{e}\Delta t \\ &- (AN(t) + BN(t)^2 + CN(t)^3)\Delta t \\ &- \frac{G_N(N(t)-N_t)(E_1^2+E_2^2)(t)}{1+\epsilon(E_1^2+E_2^2)(t)}\Delta t, \end{aligned} \tag{B3}$$

where X_1 and X_2 are independent Gaussian numbers with zero mean and standard deviation equal to 1. To maintain the continuous and unbounded character of the phase within each modulation period, and taking into account that the numerical evaluation of the arctangent function gives values between $-\pi/2$ and $\pi/2$, we have to detect the number of times that the trajectory crosses the vertical axis ($E_1 = 0$) of the complex plane and the clockwise or counterclockwise character of these crossings. If the initial

condition is such that $E_1(0) > 0$, the value of the phase at t is calculated by use of

$$\phi(t) = \arctan\left(\frac{E_2(t)}{E_1(t)}\right) + (n-m)\pi, \tag{B4}$$

where n is the total number of counterclockwise crossings (from quadrant 1, Q1, to quadrant 2, Q2, and from quadrant 3, Q3, to quadrant 4, Q4) observed until time t. In the same way, m is the total number of clockwise crossings (from Q2 to Q1 and from Q4 to Q3) observed until time t. In the opposite case, $E_1(0) < 0$, the value of the phase at t is found from

$$\phi(t) = \arctan\left(\frac{E_2(t)}{E_1(t)}\right) + (n-m+1)\pi. \tag{B5}$$

The previous algorithm has to be modified if we also want to consider the diagonal crossings: from Q1 to Q3, from Q3 to Q1, from Q2 to Q4, and from Q4 to Q2. If we consider that it is equally probable to increase or to decrease the angle in these transitions, we modify the previous algorithm by adding or subtracting π with probability 1/2 each time one of the previous crossings is observed from t to $t + \Delta t$. We use this modified algorithm to obtain the results in this work. We note, however, that the effect of considering these diagonal crossings is much smaller than that obtained when we consider only crossings from Q1 to Q2 or from Q3 to Q4, and vice versa, because the diagonal crossings are just a very small percentage of the total crossings of the vertical axis. For instance, the relative error of the final value of the variance in Fig. 2(b) when we use only Eqs. (B4) and (B5) with respect to the result found with the modified algorithm is smaller than 1% for the case $\Delta t = 10^{-5}$ ps.

APPENDIX C: CALCULATION OF THE PHASE VARIANCE AT THE STEADY STATE BELOW THE THRESHOLD

Our departure equations are Eq. (7) and a simplified version of Eq. (8) in which linearized recombination of carriers has been considered:

$$\frac{dN}{dt} = \frac{I}{e} - \frac{N}{\tau_n} - \frac{G_N(N-N_t)\mid E\mid^2}{1+\epsilon\mid E\mid^2}, \tag{C1}$$

where τ_n is the carrier lifetime. We also consider the situation in which $\alpha = 0$. We make these approximations to obtain simple analytical expressions. They do not affect the main result in this appendix—that is, to show in an alternative way the divergence of the optical phase. When the bias current, I, is below the threshold, $\mid E\mid^2$ can be ignored and Eqs. (7) and (8) are written as

$$\frac{dE_i}{dt} = a(t)E_i + \sqrt{\frac{\beta B}{2}}N\xi_i(t), \tag{C2}$$

$$\frac{dN}{dt} = \frac{I}{e} - \frac{N}{\tau_n}, \tag{C3}$$

where $a(t) = (G_N(N(t)-N_t) - 1/\tau_p)/2$ and $i = 1, 2$. The solution of Eq. (C3) is as follows:

$$N(t) = \left(N(0) - \frac{\tau_n I}{e}\right)e^{-t/\tau_n} + \frac{\tau_n I}{e}. \tag{C4}$$

The solution of Eq. (C2) is given by [53]

$$E_i(t) = h_i(t)\exp\left(\int_0^t a(s)ds\right), \tag{C5}$$

where

$$h_i(t) = E_i(0) + \sqrt{\frac{\beta B}{2}}\int_0^t N(t')\exp\left(-\int_0^{t'} a(s)ds\right)\xi_i(t')dt'. \tag{C6}$$

$h_i(t)$ are independent Gaussian processes with $< h_i(t) >= E_i(0)$ and variance $\sigma_i^2 =< h_i^2(t) > - < h_i >^2$, given by

$$\sigma_i^2 = \frac{\beta B}{2}\int_0^t N^2(t')\exp\left(-2\int_0^{t'} a(s)ds\right)dt'. \tag{C7}$$

The photon number is given by

$$P(t) = E_1^2(t) + E_2^2(t) = \left[h_1^2(t) + h_2^2(t)\right]\exp\left(2\int_0^t a(s)ds\right). \tag{C8}$$

$P(t)$ is an exponential process because $h_i(t)$ are independent Gaussian processes. The exponential process is determined by just one parameter, $< P(t) >$, which is calculated by averaging Eq. (C8). A simplified expression for $< P(t) >$ can be obtained by considering the evolution at times long enough for N to reach a constant value; that is, $t >> \tau_n$, $N(t) \approx \tau_n I/e = \bar{N}$, and $a(t) \approx [G_N(\bar{N} - N_t) - 1/\tau_p]/2 = \bar{a}$, where $\bar{a} < 0$ since $I < I_{\rm th}$. Equation (C8) then reads

$$P(t) \approx \left[h_1^2(t) + h_2^2(t)\right]e^{2\bar{a}t}, \tag{C9}$$

with an average value given by

$$< P(t) > \approx P(0) + \frac{\beta B\bar{N}^2}{2\mid\bar{a}\mid}\left(1 - e^{2\bar{a}t}\right), \tag{C10}$$

which becomes independent of time when $t >> 1/2\mid\bar{a}\mid$. In the long-time regime, $P(t)$ becomes an exponential random variable, P, with statistical properties independent of time, with an average given by $\approx P(0) + \beta B\bar{N}^2/2\mid\bar{a}\mid$.

We now discuss the evolution of the phase by using Eq. (A12), which for $\alpha = 0$ reads

$$d\phi = \sqrt{\frac{\beta B}{2P}} N dW_\phi. \tag{C11}$$

Integration of this equation gives

$$\phi(t) = \phi(0) + \sqrt{\frac{\beta B}{2}} \int_0^t N(t) \sqrt{\frac{1}{P(t)}} dW_\phi. \tag{C12}$$

Assuming that $t >> \tau_n$ and $t >> 1/2 \mid \bar{a} \mid$, we can approximate $N(t) \approx \bar{N}$ and $P(t) \approx P$ so

$$\phi(t) \approx \sqrt{\frac{\beta B}{2}} \bar{N} \sqrt{\frac{1}{P}} \int_0^t dW_\phi, \tag{C13}$$

where for simplicity we assume that $\phi(0) = 0$. The previous integral is $W_\phi(t)$, a Wiener process with zero mean and variance given by $V[W_\phi(t)] = t$. In this way, we have expressed the phase as $\phi(t) = \gamma \sqrt{1/P} W_\phi(t)$, where $\gamma = \sqrt{\beta B/2} \bar{N}$ and where $\sqrt{1/P}$ and $W_\phi(t)$ are statistically independent because $F_P(t)$ and $F_\phi(t)$ are independent. Applying the formula of the variance of the product of two statistically independent random variables, we find that the variance of the phase is given by

$$\sigma_\phi^2(t) \approx \gamma^2 < \frac{1}{P} > t = \gamma^2 t \int_0^\infty \frac{e^{-P/}}{P} dP. \tag{C14}$$

The divergence of the phase variance lies in the fact that this integral has a logarithmic divergence.

[1] F. Xu, X. Ma, Q. Zhang, H.-K. Lo, and J.-W. Pan, Secure quantum key distribution with realistic devices, Rev. Mod. Phys. **92**, 025002 (2020).

[2] T. K. Paraïso, R. I. Woodward, D. G. Marangon, V. Lovic, Z. Yuan, and A. J. Shields, Advanced laser technology for quantum communications (tutorial review), Adv. Quantum Technol. **4**, 2100062 (2021).

[3] M. Stipčević and Ç. K. Koç, in *Open Problems in Mathematics and Computational Science* (Springer, 2014), p. 275.

[4] X. Ma, X. Yuan, Z. Cao, B. Qi, and Z. Zhang, Quantum random number generation, npj Quantum Inf. **2**, 1 (2016).

[5] M. Herrero-Collantes and J. C. Garcia-Escartin, Quantum random number generators, Rev. Mod. Phys. **89**, 015004 (2017).

[6] V. Mannalath, S. Mishra, and A. Pathak, A comprehensive review of quantum random number generators: Concepts, classification and the origin of randomness, (2022), arXiv preprint ArXiv:2203.00261.

[7] A. Stefanov, N. Gisin, O. Guinnard, L. Guinnard, and H. Zbinden, Optical quantum random number generator, J. Mod. Opt. **47**, 595 (2000).

[8] T. Jennewein, U. Achleitner, G. Weihs, H. Weinfurter, and A. Zeilinger, A fast and compact quantum random number generator, Rev. Sci. Instrum. **71**, 1675 (2000).

[9] W. Wei and H. Guo, Bias-free true random-number generator, Opt. Lett. **34**, 1876 (2009).

[10] H. Guo, W. Tang, Y. Liu, and W. Wei, Truly random number generation based on measurement of phase noise of a laser, Phys. Rev. E **81**, 051137 (2010).

[11] Y. Shen, L. Tian, and H. Zou, Practical quantum random number generator based on measuring the shot noise of vacuum states, Phys. Rev. A **81**, 063814 (2010).

[12] B. Qi, Y.-M. Chi, H.-K. Lo, and L. Qian, High-speed quantum random number generation by measuring phase noise of a single-mode laser, Opt. Lett. **35**, 312 (2010).

[13] M. Jofre, M. Curty, F. Steinlechner, G. Anzolin, J. Torres, M. Mitchell, and V. Pruneri, True random numbers from amplified quantum vacuum, Opt. Express **19**, 20665 (2011).

[14] A. Argyris, E. Pikasis, S. Deligiannidis, and D. Syvridis, Sub-Tb/s physical random bit generators based on direct detection of amplified spontaneous emission signals, J. Lightwave Technol. **30**, 1329 (2012).

[15] F. Xu, B. Qi, X. Ma, H. Xu, H. Zheng, and H.-K. Lo, Ultrafast quantum random number generation based on quantum phase fluctuations, Opt. Express **20**, 12366 (2012).

[16] C. Abellán, W. Amaya, M. Jofre, M. Curty, A. Acín, J. Capmany, V. Pruneri, and M. Mitchell, Ultra-fast quantum randomness generation by accelerated phase diffusion in a pulsed laser diode, Opt. Express **22**, 1645 (2014).

[17] Z. Yuan, M. Lucamarini, J. Dynes, B. Fröhlich, A. Plews, and A. Shields, Robust random number generation using steady-state emission of gain-switched laser diodes, Appl. Phys. Lett. **104**, 261112 (2014).

[18] D. G. Marangon, A. Plews, M. Lucamarini, J. F. Dynes, A. W. Sharpe, Z. Yuan, and A. J. Shields, Long-term test of a fast and compact quantum random number generator, J. Lightwave Technol. **36**, 3778 (2018).

[19] B. Septriani, O. de Vries, F. Steinlechner, and M. Gräfe, Parametric study of the phase diffusion process in a gain-switched semiconductor laser for randomness assessment in quantum random number generator, AIP Adv. **10**, 055022 (2020).

[20] R. Shakhovoy, D. Sych, V. Sharoglazova, A. Udaltsov, A. Fedorov, and Y. Kurochkin, Quantum noise extraction from the interference of laser pulses in an optical quantum random number generator, Opt. Express **28**, 6209 (2020).

[21] R. Shakhovoy, V. Sharoglazova, A. Udaltsov, A. Duplinskiy, V. Kurochkin, and Y. Kurochkin, Influence of chirp, jitter, and relaxation oscillations on probabilistic properties of laser pulse interference, IEEE J. Quantum Electron. **57**, 1 (2021).

[22] C. Abellan, W. Amaya, D. Domenech, P. Muñoz, J. Capmany, S. Longhi, M. W. Mitchell, and V. Pruneri, Quantum entropy source on an InP photonic integrated circuit for random number generation, Optica **3**, 989 (2016).

[23] V. Lovic, D. G. Marangon, M. Lucamarini, Z. Yuan, and A. J. Shields, Characterizing Phase Noise in a Gain-Switched

Laser Diode for Quantum Random-Number Generation, Phys. Rev. Appl. **16**, 054012 (2021).
[24] A. Quirce and A. Valle, Phase diffusion in gain-switched semiconductor lasers for quantum random number generation, Opt. Express **29**, 39473 (2021).
[25] M. Lax, Quantum noise. IV. quantum theory of noise sources, Phys. Rev. **145**, 110 (1966).
[26] M. Lax and W. Louisell, Quantum noise. XII. density-operator treatment of field and population fluctuations, Phys. Rev. **185**, 568 (1969).
[27] H. Risken, in *The Fokker-Planck Equation* (Springer, 1996).
[28] C. H. Henry and R. F. Kazarinov, Quantum noise in photonics, Rev. Mod. Phys. **68**, 801 (1996).
[29] F. Arecchi, V. Degiorgio, and B. Querzola, Time-Dependent Statistical Properties of the Laser Radiation, Phys. Rev. Lett. **19**, 1168 (1967).
[30] L. A. Coldren, S. W. Corzine, and M. L. Mashanovitch, *Diode Lasers and Photonic Integrated Circuits* Vol. 218 (John Wiley & Sons, New York, 2012).
[31] G. P. Agrawal and N. K. Dutta, *Semiconductor Lasers* (Springer Science & Business Media, Berlin/Heidelberg, 2013).
[32] P. Spano, S. Piazzolla, and M. Tamburrini, Phase noise in semiconductor lasers: A theoretical approach, IEEE J. Quantum Electron. **19**, 1195 (1983).
[33] N. Schunk and K. Petermann, Noise analysis of injection-locked semiconductor injection lasers, IEEE J. Quantum Electron. **22**, 642 (1986).
[34] C. Henry, Phase noise in semiconductor lasers, J. Lightwave Technol. **4**, 298 (1986).
[35] K. Petermann, *Laser Diode Modulation and Noise* Vol. 3 (Springer Science & Business Media, Berlin/Heidelberg, 1991).
[36] S. Balle, P. Colet, and M. San Miguel, Statistics for the transient response of single-mode semiconductor laser gain switching, Phys. Rev. A **43**, 498 (1991).
[37] S. Balle, F. De Pasquale, N. Abraham, and M. San Miguel, Statistics of the transient frequency modulation in the switch-on of a single-mode semiconductor laser, Phys. Rev. A **45**, 1955 (1992).
[38] C. W. Gardiner, *et al.*, *Handbook of Stochastic Methods* Vol. 3 (Springer, Berlin, 1985).
[39] R. Shakhovoy, M. Puplauskis, V. Sharoglazova, A. Duplinskiy, D. Sych, E. Maksimova, S. Hydyrova, A. Tumachek, Y. Mironov, V. Kovalyuk, A. Prokhodtsov, G. Goltsman, and Y. Kurochkin, Phase randomness in a semiconductor laser: Issue of quantum random number generation, Phys. Rev. A **107**, 012616 (2023).
[40] A. Quirce and A. Valle, Spontaneous emission rate and phase diffusion in gain-switched laser diodes, Opt. Laser Technol. **150**, 107992 (2022).
[41] V. Lovic, D. Marangon, M. Lucamarini, Z. Yuan, and A. Shields, in *CLEO: QELS_Fundamental Science* (Optica Publishing Group, 2022), p. FTu4A.
[42] M. P. Lévy, Le mouvement brownien plan, Am. J. Math. **62**, 487 (1940).
[43] A. Rosado, A. Pérez-Serrano, J. M. G. Tijero, A. Valle, L. Pesquera, and I. Esquivias, Numerical and experimental analysis of optical frequency comb generation in gain-switched semiconductor lasers, IEEE J. Quantum Electron. **55**, 2001012 (2019).
[44] A. Valle, in *Photonics*, Vol. 8 (Multidisciplinary Digital Publishing Institute, 2021), p. 388.
[45] P. E. Kloeden and E. Platen, in *Numerical Solution of Stochastic Differential Equations* (Springer, 1992).
[46] S. Balle, N. B. Abraham, P. Colet, and M. San Miguel, Parametric dependence of stochastic frequency variations in the gain switching of a single-mode laser diode, IEEE J. Quantum Electron. **29**, 33 (1993).
[47] A. Quirce, A. Rosado, J. Díez, A. Valle, A. Pérez-Serrano, J.-M. G. Tijero, L. Pesquera, and I. Esquivias, Nonlinear dynamics induced by optical injection in optical frequency combs generated by gain-switching of laser diodes, IEEE Photonics J. **12**, 1 (2020).
[48] T. Pham-Gia, N. Turkkan, and E. Marchand, Density of the ratio of two normal random variables and applications, Commun. Stat. Theory Methods **35**, 1569 (2006).
[49] F. Spitzer, Some theorems concerning 2-dimensional Brownian motion, Trans. Am. Mac. Soc. **87**, 187 (1958).
[50] J. Hannay and M. Wilkinson, Mean square winding angle of Brownian motion around an impenetrable cylinder, J. Phys. A: Math. Theor. **55**, 234007 (2022).
[51] C. Abellán Sánchez, Quantum random number generators for industrial applications, PhD Thesis (2018).
[52] C. Gardiner and P. Zoller, *Quantum Noise: A Handbook of Markovian and Non-Markovian Quantum Stochastic Methods with Applications to Quantum Optics* (Springer Science & Business Media, Berlin/Heidelberg, 2004).
[53] A. Valle, M. Rodriguez, and C. R. Mirasso, Analytical calculation of timing jitter in single-mode semiconductor lasers under fast periodic modulation, Opt. Lett. **17**, 1523 (1992).